Cyclovirobuxine D pretreatment ameliorates septic heart injury through mitigation of ferroptosis

JIANXIN WANG[1*], PENG GUAN[1,2*], YU CHEN[1], MENG XU[1], NA WANG[1] and ENSHENG JI[1]

[1]Department of Physiology, School of Pharmacy, Hebei University of Chinese Medicine, Shijiazhuang, Hebei 050091; [2]College of Life Science, Hebei Normal University, Shijiazhuang, Hebei 050024, P.R. China

Received February 22, 2023; Accepted June 1, 2023

DOI: 10.3892/etm.2023.12106

Abstract. Myocardial dysfunction is a frequent complication in patients with severe sepsis. However, effective drugs for the prevention of myocardial dysfunction and the molecular mechanisms of the disease remain elusive. The present study demonstrated that Cyclovirobuxine D (CVB-D) could improve cardiac dysfunction in a cecal ligation and puncture (CLP) model in rodents and in a lipopolysaccharide (LPS) model *in vitro*. Echocardiography and histopathological examination were used to detect changes in cardiac structure and function. Kits were used to detect indicators of cardiac injury, transmission electron microscopy to detect structural changes in mitochondria and reverse transcription-quantitative PCR to detect prostaglandin-endoperoxide synthase 2 and hamp expression levels. L-Glutathione and malondialdehyde levels and superoxide dismutase activity were measured using kits. Cell viability was measured with the Cell Counting Kit-8. Iron metabolism-related proteins, inflammatory factor levels and related pathway proteins were detected using western blot analysis. Changes in L-type calcium currents were detected by membrane clamp, and contractility of cardiomyocytes was measured by Ion Optix. CVB-D attenuated CLP-induced cardiac malfunction in septic rats, with changes observed in myocardial pathological structure, creatine kinase isoenzyme (CK-MB), lactate dehydrogenase (LDH) and cardiac troponin I (cTnI). CVB-D attenuated sepsis-induced lipid peroxidation and iron overload. In addition, CVB-D decreased the expression of CK-MB, LDH and cTnI, suppressed oxidative stress index levels and reduced the production of reactive oxygen species. CVB-D decreased LPS-induced cytoplasmic iron overload by increasing upregulation of iron uptake molecules. Conversely, CVB-D significantly increased the upregulation of ferroportin 1. CVB-D pretreatment significantly reduced the levels of hamp mRNA compared with the LPS-treated group. CVB-D pretreatment significantly reduced inflammatory factor levels and the ratio of phosphorylated vs. total signal transducer and activator of transcription 3. The expression of SLC7A11 and GPX4 was upregulated in septic cells pretreated with CVB-D, however treatment with ML385 largely decreased this upregulation. Of note, CVB-D inhibited the inward flow of calcium ions through the LTCC. In conclusion, these findings suggest that CVB-D alleviated sepsis-induced cardiac iron toxicity by alleviating iron metabolism.

Correspondence to: Professor Na Wang or Professor Ensheng Ji, Department of Physiology, School of Pharmacy, Hebei University of Chinese Medicine, 326 Xinshi South Road, Shijiazhuang, Hebei 050091, P.R. China
E-mail: wangna9503@126.com
E-mail: jesphy@126.com

*Contributed equally

Abbreviations: CVB-D, cyclovirobuxine D; CLP, cecal ligation and puncture; LPS, lipopolysaccharide; CK-MB, creatine kinase isoenzyme; LDH, lactate dehydrogenase; cTnI, cardiac troponin I; DMT1, divalent metal transporter 1; TfR1, transferrin receptor 1; LTCCs, L-type Ca^{2+} channels; FPN1, ferroportin 1; SC, septic cardiomyopathy; SD, Sprague Dawley; H&E, hematoxylin and eosin; SOD, superoxide dismutase; GSH, glutathione; MDA, malondialdehyde; EF, ejection fraction; FS, fractional shortening; LVESV, left ventricular end-systolic volume; LVEDV, left ventricular end-diastolic volume; CCK-8, Cell Counting Kit-8; Calcein-AM, calcein-acetoxymethyl ester; PTGS2, prostaglandin-endoperoxide synthase 2; DCFH-DA, 2',7'-dichlorofluorescein diacetate; VER, verapamil; I-V, current-voltage; FtH, ferritin heavy chain; Ferr-1, ferrostatin-1; ROS, reactive oxygen species; SLC7A11, solute carrier family 7 member 11; SLC3A2, solute carrier family member 2; Nrf2, nuclear factor erythroid 2-related factor 2; IL, interleukin; TNF-α, tumor necrosis factor-α; STAT3, signal transducer and activator of transcription 3; GPX4, glutathione peroxidase 4; gprot, g protein; $I_{Ca\text{-}L}$, L-type Ca^{2+} currents; HBSS, Hank's balanced salt solution; AMPK, adenosine 5'-monophosphate-activated protein kinase

Key words: cyclovirobuxine D, septic cardiomyopathy, ferroptosis, iron, nuclear factor erythroid 2-related factor 2, L-type Ca^{2+} channels

Introduction

Septic cardiomyopathy (SC), with mortality rates of up to 70%, is considered the primary cause of death in sepsis (1). Since clinicians have recognized that the myocardium is functionally and structurally damaged in patients with SC (2), its prevention and treatment measures have become a popular research topic. There is currently no consensus on the mechanism of SC (3). Cytokines, pathogen-associated molecular patterns, endogenous damage-associated molecular patterns, oxidative

stress, changes in nitric oxide metabolism and mitochondrial dysfunction have been individually proposed to lead to SC through different pathways (4-6). However, the majority of treatments targeting specific cytokines have failed in clinical trials (7). Further investigation of novel molecular targets and effective therapeutic approaches involved in SC continues to be of great interest.

Iron is essential to life because it is involved in numerous biological processes, such as energy metabolism and nucleotide synthesis and repair (8). However, iron overload can affect normal cellular functions through increasing oxidative stress or directly inducing ferroptosis by catalyzing the oxidation of phospholipids in the cell membrane (9). Ferroptosis is a form of programmed cell death, which is usually accompanied by a large amount of iron accumulation and lipid peroxidation (10). A previous study reported that iron chelators could suppress the generation of radicals and protect against damage in experimental sepsis (11). Moreover, a recent study reported that ferroptosis is an important process, which mediates the pathogenesis and progression of sepsis-induced cardiomyopathy (12). Similarly, it has been previously reported that ferroptosis could be suppressed by dexmedetomidine to alleviate septic heart injury (13). These results suggest that negative regulation of sepsis-induced iron concentration and ferroptosis could be beneficial for treatment of sepsis-induced cardiac injury.

Cyclovirobuxine D (CVB-D) is a triterpenoid alkaloid extracted from the traditional Chinese medicinal plant Buxus microphylla, which has been widely used to treat a number of cardiovascular diseases in China (14). Previous studies have suggested that that CVB-D may play an important protective role in the cardiovascular system by activating the Nrf2 signaling pathway to inhibit oxidative stress, or by suppressing the accumulation of reactive oxygen species and inflammation levels (15-17). However, it is unclear whether CVB-D has a protective effect against myocardial injury in sepsis. In the present study, whether CVB-D had a cardioprotective effect during sepsis was assessed with a focus on revealing the underlying mechanisms of action.

Materials and methods

Animal treatment. Experiments were performed on 8-week-old male Sprague Dawley (SD) rats (weight, 180-220 g; Rong Heng Biological Co., Ltd). A total of 30 SD rats were randomly assigned to five rat cages (n=6/cage) after one week of acclimation, feeding in an indoor animal room with a 12 h light/dark cycle, a temperature of 22±2˚C and 40-60% relative humidity with free access to food and water. All procedures were performed with the approval of the Animal Care and Use Committee of Hebei University of Chinese Medicine (approval no. DWLL202206006).

Animal experiments were performed based on scientific rationale according to the 3R principles of animal experimentation. To reduce pain in rats, pentobarbital sodium was used as an anesthetic during surgery. The rats were randomized into five groups (n=6/group) as follows: Control group, CLP group, CLP + CVB-D group, CVB-D group and CLP + Ferr-1 (Ferrostatin-1, ferroptosis inhibitor) group. CLP surgery was performed to induce septic cardiac dysfunction. CVB-D was dissolved in methanol (final concentration, 10 mM) and stored at 4˚C as a stock solution. CVB-D (cumulative dose of 4 mg/kg; Meilunbio Co., Ltd.) (11) or saline was administered by gavage in rats for four consecutive days before CLP surgery. The rats received an intraperitoneal injection of Ferr-1 (2 μmol/kg; Xcess Biosciences) or saline once daily for four days before surgery.

The CLP surgery was performed as described previously (18). Briefly, rats were anesthetized by intraperitoneal injection of pentobarbital sodium (40 mg/kg) then fixed on an operating table and incised 1.5 cm along the midline of the abdomen under aseptic conditions. After the colon of the rat was exposed and ligated at 1/2 to the root, the distal cecum was then punctured twice with a 9-gauge needle. A small volume of fecal contents from the punctured cecum was spilled into the abdominal cavity. The control group underwent the same surgical procedure, but without cecal puncture. All animals were placed on the operating table and immobilized with ketamine (40 mg/kg; intramuscular injection in the front of the thigh) and xylazine (10 mg/kg; intraperitoneally administered) anesthesia, after which 5 ml blood was obtained from the abdominal aorta. After rats were sacrificed by exsanguination from the carotid artery, blood, heart and liver tissues were obtained, rats were sacrificed by exsanguination from the carotid artery. Blood (centrifuged at 3,000 x g for 15 min at 4˚C) was collected to obtain serum for measuring cardiac function biomarker levels. After the hearts were isolated, tissue samples from each heart were used for hematoxylin and eosin (H&E) staining, transmission electron microscopy (TEM), reverse transcription-quantitative PCR (RT-qPCR) and biochemistry testing. Liver samples were also collected for RT-qPCR.

Histopathological examination. Heart tissues were soaked in 4% paraformaldehyde at 4˚C for two days, then the tissue samples were gradually dehydrated in an ascending gradient of ethanol 30 min each at room temperature, embedded in paraffin and cut into 4 μm sections. Slides were stained with H&E 5 min each at room temperature and observed under a light microscope (Leica Microsystems GmbH).

Detection of cardiac injury markers. Biochemical indicators of myocardial injury and lipid peroxidation were detected by creatine kinase-muscle and brain (CK-MB; cat. no. H197-1-1; Nanjing Jiancheng Institute of Bioengineering), lactate dehydrogenase (LDH; cat. no. A020-2-2; Nanjing Jiancheng Institute of Bioengineering) and cardiac troponin I (cTnI; cat. no. H149-2; Nanjing Jiancheng Institute of Bioengineering) content in serum, as well as malondialdehyde (MDA; cat. no. A003-1-1; Nanjing Jiancheng Institute of Bioengineering), superoxide dismutase (SOD; cat. no. A001-3-2; Nanjing Jiancheng Institute of Bioengineering) and reduced glutathione (GSH; cat. no. A006-2-1; Nanjing Jiancheng Institute of Bioengineering) content in tissue. The content and activity of each sample indicator was measured spectrophotometrically using biochemical detection kits (Nanjing Jiancheng Bioengineering Institute).

Echocardiography. Cardiac function was examined in rats 24 h after CLP. Rats were anesthetized by inhalation 2.5% isoflurane in 5% carbon dioxide and 95% oxygen and their chest fur removed with depilation cream (cat. no. VT-200; Veet; Reckitt Benckiser). A coupling agent (Kofu Medical Technology Development Co., Ltd) was applied evenly to the skin then M-mode echocardiograms were recorded and analyzed using high-frequency echocardiography (Vevo 2100, VisualSonics, Inc.). Left ventricular ejection fraction (EF), fractional shortening (FS), left ventricular end-systolic volume (LVESV) and left ventricular end-diastolic volume (LVEDV) were measured.

Transmission electron microscopy. Cardiac tissue samples were cut into 1 mm cubes and fixed in 2.5% glutaraldehyde in 0.1 M phosphate buffer for at least 24 h at room temperature. All samples were postfixed in 1% osmium tetroxide for 2 h at room temperature, dehydrated in an ascending acetone gradient, embedded in Epon 812 for 72 h at 60˚C, cut into 70 nm-thick sections, mounted and double-stained with uranyl acetate and lead citrate for 20 min at room temperature. The samples were then imaged using a transmission electron microscope (H-7600; Hitachi, Ltd.).

RT-qPCR. H9C2 cells were collected and pooled together to achieve sufficient RNA. TRIzol (cat. no. RR047A; Takara Bio, Inc.) total RNA extraction reagent was used for RNA extraction and a PrimeScript™ RT reagent kit (cat. no. RR047A; Takara Bio, Inc.) was used to synthesize cDNA according to the manufacture's protocol. Detection of the mRNA expression levels of the hepcidin gene (hamp) was performed against GAPDH (19). The following thermocycling conditions were used for PCR: R67 Initial denaturation stage, 95˚C for 5 min. Cycling stages were as follows: Denaturation, 95˚C for 30 sec; annealing, 60˚C for 30 sec; and extension, 72˚C for 30 sec, for a total of 40 cycles. Final extension stage: 72˚C for 5 min. Relative mRNA expression levels were determined using the $2^{-\Delta\Delta Cq}$ method (20). The primers sequences used were as follows: Hamp forward (F), 5'-CCTGAGCAGCGGTGCCTATC-3' and reverse (R), 5'-TGGTGTCTCGCTTCCTTCGC-3'; Prostaglandin-endoperoxide synthase 2 (Ptgs2) F, 5'-ATGTTCGCATTCTTTGCCCAG-3' and R, 5'-TACACCTCTCCACCGATGAC-3'; and GAPDH F, 5'-GAGTCAACGGATTTGGTCGT-3' and R, 5'-GACAAGCTTCCCGTTCTCAG-3'.

Tissue iron measurements. Non-heme levels of iron in the heart were measured. Samples of heart tissue weighing ~50 mg were obtained then incubated with 10 times the volume of tissue digestive liquid (3M hydrochloric acid + 0.61M trichloroacetic acid) for 60 h at 65˚C. After centrifugation (3,000 x g for 15 min at 4˚C), the supernatant was collected for spectrophotometric quantification of the formation of the Fe(II)-bathophenanthroline disulfonate complex. Supernatant (0.5 ml) was added to 1.5 ml of iron chromogen and boiled in a water bath for 5 min. Iron developing color working solution (cat. no. A039-1-1; Nanjing Jiancheng Bioengineering Institute) was freshly prepared and the absorbance was measured at 535 nm. A standard curve was generated and the non-heme iron content of samples was calculated according to a formula provided by the manufacturer.

Cell culture. H9C2 cardiomyoblasts purchased from Procell Life Science & Technology Co., Ltd. were cultured in DMEM (cat. no. C11995500BT; Gibco; Thermo Fisher Scientific, Inc.) supplemented with 10% fetal bovine serum (cat. no. 10270106; Gibco; Thermo Fisher Scientific, Inc.) and 1% penicillin-streptomycin in an incubator with a 5% CO_2 atmosphere at 37˚C. Cell culture medium was changed every other day. A stock solution of CVB-D (final concentration, 10 mM) (cat. no. 860-79-7; Meilunbio Co., Ltd.) was prepared in methanol. Cells were pretreated with CVB-D at doses of 0.1, 1, 10 or 100 μmol/l at 37˚C for 24 h, while the control groups were treated with an equivalent volume of PBS. To establish a model of septic myocardial injury *in vitro*, H9C2 cells were incubated at 37˚C for 12 h with LPS at doses of 0.1, 1, 10 or 100 μg/ml (Shanghai Aladdin Biochemical Technology Co., Ltd.) (21). Cells were then harvested for analysis.

Cell Counting Kit-8 (CCK-8) assay. The proliferation capacity of the cells was assessed in a 96-well plate ($2x10^5$ cells/well) using the CCK-8 assay (22). The cells were incubated in 96-well plates overnight before the addition of CCK-8. After stimulation with CVB-D or LPS (cat. no. 93572-42-0; MilliporeSigma) for 24 h, 10 μl of CCK-8 reagent was added and incubated for 2 h at 37˚C under dark conditions. The absorbance value at 450 nm of each well was recorded with a microplate reader.

Detection of H9C2 reactive oxygen species (ROS) generation. The level of fluorescence produced by the fluorescent probe 2',7'-dichlorofluorescein diacetate (DCFH-DA; cat. no. S0033S; Beyotime Institute of Biotechnology) was used to quantify ROS generation. Groups of H9C2 cells were loaded with 1:1,000 DCFH-DA probes diluted with serum-free medium and incubated for 20 min in a 37˚C cell incubator after 24 h of administration. DCFH-DA is hydrolyzed into dichlorodihydrofluorescein (DCFH) after entering the membrane of the H9C2 cell. DCFH, which is not fluorescent, can be oxidized by intracellular ROS to fluorescent DCF. The level of ROS was detected according to the fluorescence intensity. The fluorescence intensity was imaged using a fluorescence microscope (IX73; Olympus Corporation) and quantified using ImageJ (version 1.5.1) software (National Institutes of Health).

Quenching of calcein fluorescence by the intracellular labile iron pool. Intracellular labile iron was quantified using calcein-acetoxymethyl ester (Calcein-AM) (23). Cellular cytoplasmic esterase converts a nonfluorescent acetoxy ester fraction, Calcein-AM, into fluorescent calcein, which is impenetrable to other cells. When iron binds to calcein, its fluorescence is quenched and then restored when the iron loses its stronger chelating agent. Cells were incubated in 24-well plates at 37˚C for 24 h. Then CVB-D or LPS was given to incubate for 24 h. Calcein-AM (cat. no. 40719ES50; Shanghai Yeasen Biotechnology Co., Ltd.) was added to cells in a 24-well plate at a final concentration of 0.25 μM and incubated for 30 min at 37˚C. The fluorescence level was then measured using an inverted fluorescence microscope at the excitation and emission wavelengths of 488 and 525 nm, respectively (IX73; Olympus Corporation).

Western blot analysis. As previously described (24), total protein in myocardial tissue and H9C2 cells were precipitated in RIPA lysis buffer solution (cat. no. SL1020; Coolaber, Ltd.) containing protease inhibitors. Tissue and cells were centrifuged at 4˚C for 20 min at 12,000 x g to remove the insoluble residue. The supernatant was removed and the concentration of total protein was determined using a BCA kit (cat. no. CW0014; Beijing Kangwei Century Biotechnology Co., Ltd.). Equal amounts of total protein were separated by electrophoresis using 10 or 12% gel. Separated proteins were subsequently transferred to polyvinylidene fluoride (EMD Millipore) membranes and blocked overnight at 37˚C with TBS-0.1% Tween 20 in 5% skimmed milk. Membranes were incubated with GPX4 (1:2,000; cat. no. ET1706-45; HUABIO), SLC7A11 (1:1,000; cat. no. DF12509; Affinity Biosciences), transferrin receptor 1 (TfR1; 1:2,000; cat. no. abs131442; Absin), ferroportin 1 (FPN1; 1:3,000; cat. no. GTX100573; Absin), divalent metal transporter 1 (DMT1; 1:2,000; cat. no. abs112967; Absin), ferritin heavy chain (FtH; 1:1,000; cat. no. AB183781; Abcam), IL-6 (1:1,000; cat. no. GB11117; Wuhan Servicebio Technology Co., Ltd.), IL-1β (1:1,000; cat. no. AF5103; Affinity Biosciences), tumor necrosis factor-α (TNF-α; 1:1,000; cat. no. AF7014; Affinity Biosciences), phosphorylated-STAT3 (p-STAT3; 1:1,000; cat. no. AF3294; Affinity Biosciences), STAT3 (1:1,000; cat. no. AF6293; Affinity Biosciences), Nrf2 (1:1,000; cat. no. M200-3; MBL International Co.), Lamin B1 (1:1,500; cat. no. SI17-06; HUABIO) and β-tubulin (1:2,000; cat. no. A01857-1; Wuhan Boster Biological Technology, Ltd.) antibodies primary antibodies at 4˚C overnight. Goat anti-rabbit IgG (H+L)-HRP (1:10,000; cat. no. S0001) or goat anti-mouse IgG(H+L)-HRP (1:1,000; cat. no. S0002; both from Affinity Biosciences) were then placed at room temperature for 2 h. The cell membranes were then washed again and Visioncapt (V16.12; Vilber Lourmat) was used for quantification.

Measurement of Ca^{2+} concentration by fluo-4 AM staining. The concentration of Ca^{2+} was assessed using a Fluo-4 AM kit (cat. no. F8501; Beijing Solarbio Science & Technology Co., Ltd) according to manufacturer's instructions. $1x10^5$ H9C2 cells were seeded into a 24-well plate and cultured at 37˚C for 24 h. Fluo-4 AM (1 ml, 4 μM) was added to each well and incubated in darkness at 37˚C for 20 min. Hank's Balanced Salt Solution (HBSS; cat. no. F8501; Beijing Solarbio Science & Technology Co.) containing 1% fetal bovine serum was added and incubated at 37˚C for 40 min. After being washed three times with HBSS and FBS (1 ml per well) was used each time, cells were imaged to detect fluorescent calcium ions using excitation and emission wavelengths of 494 and 516 nm, respectively, with an inverted fluorescence microscope (IX73; Olympus Corporation).

Measurement of $I_{Ca\text{-}L}$ and cell shortening. To further analyze whether CVB-D inhibits calcium inwards flow through LTCCs, a diaphragm clamp technique was utilized to detect L-type calcium current changes. With the use of L-type calcium channel inhibitors to block calcium channels, the inwards flow of calcium ions is reduced, resulting in protection against myocardial injury. Verapamil (VER) is a typical calcium channel blocker. The expression of the L-type calcium channel (LTCC) in ventricular myocytes was analyzed utilizing the whole-cell patch-clamp method. The intracellular solution consisted of tetraethylammonium chloride (cat. no. 56-34-8; TCL), $MgCl_2$ (cat. no. 10012818; Sinopharm Group Chemical Reagent Co., Ltd), $CaCl_2$ (cat. no. 10005861; Sinopharm Group Chemical Reagent Co., Ltd), Glucose (cat. no. 56-86-0; Sigma-Aldrich; Merck KGaA) and N-2-hydroxyethylpiperazine-N-ethane-sulphonicacid (cat. no. 7365-45-9, Beijing Bailingwei Technology Co., Ltd), and the extracellular solution consisted of CsCl (cat. no. 7647-17-8; Shanghai Yi En Chemical Technology Co., Ltd), tetraethylammonium chloride, ATP-Mg (cat. no. 7480-12-9; Sigma-Aldrich; Merck KGaA), N-2-hydroxyethylpiperazine-N-ethane-sulphonicacid and ethylene glycol tetraacetic acid (cat. no. 67-42-5; Sigma-Aldrich; Merck KGaA). Currents under filtered at 2 kHz were recorded with Axon patch 200 B amplifier after the cells were connected with glass electrodes (Sutter Instrument). The Axon Patch 200B amplifier analyzed the current and pCLAMP™ software (version 10.0) was used for data analysis (Molecular Devices, LLC). The contraction of myocardial cells was measured. Cells were placed on an inverted microscope (Ion Optix) platform and perfused with the external solution to induce cardiac myocyte shortening 2 msec each time of 0.5 Hz. Cardiomyocytes with clear transverse lines and in good condition were selected to measure contraction.

Statistical analysis. Experimental data are presented as the mean ± standard deviation. Data were processed using GraphPad Prism software (version 8.0; Dotmatics) using one-way ANOVA followed by Tukey's test for comparisons among multiple groups. $P<0.05$ was considered to indicate a statistically significant difference.

Results

CVB-D exerts a protective effect on LPS-treated H9C2 cells. LPS is commonly used to generate pathophysiological conditions of septic cardiomyopathy in investigation studies. CCK-8 assay results demonstrated that H9C2 cell viability was significantly reduced by LPS in a dose-dependent manner (Fig. 1A). A dose of 10 μg/ml LPS at 37˚C for 12 h was selected to induce a cellular sepsis model for further use in the present study, as previously described (21,25,26). Additionally, a CCK-8 assay was performed to assess the effects of CVB-D on H9C2 cell viability. The results demonstrated that CVB-D had no cytotoxic effect on H9C2 cells at 0.1 or 1 μM, but significantly reduced H9C2 survival at 10 and 100 μM (Fig. 1A). Therefore, a dose of 1 μM CVB-D was selected for use in the present study. Moreover, pretreatment of H9C2 cells with 1 μM CVB-D significantly enhanced LPS-damaged cell viability (Fig. 1B). As expected, LPS distinctly weakened CK-MB, LDH activity and cTnI levels ($P<0.01$), whereas the inhibitory effect was blocked by CVB-D pretreatment (Fig. 1C).

CVB-D inhibits ferroptosis in LPS-treated H9C2 cells. The effect of CVB-D on H9C2 lipid peroxidation levels and production of first line defense antioxidant enzymes GSH and SOD were also assessed. LPS treatment of H9C2 cells significantly increased production of MDA, but significantly

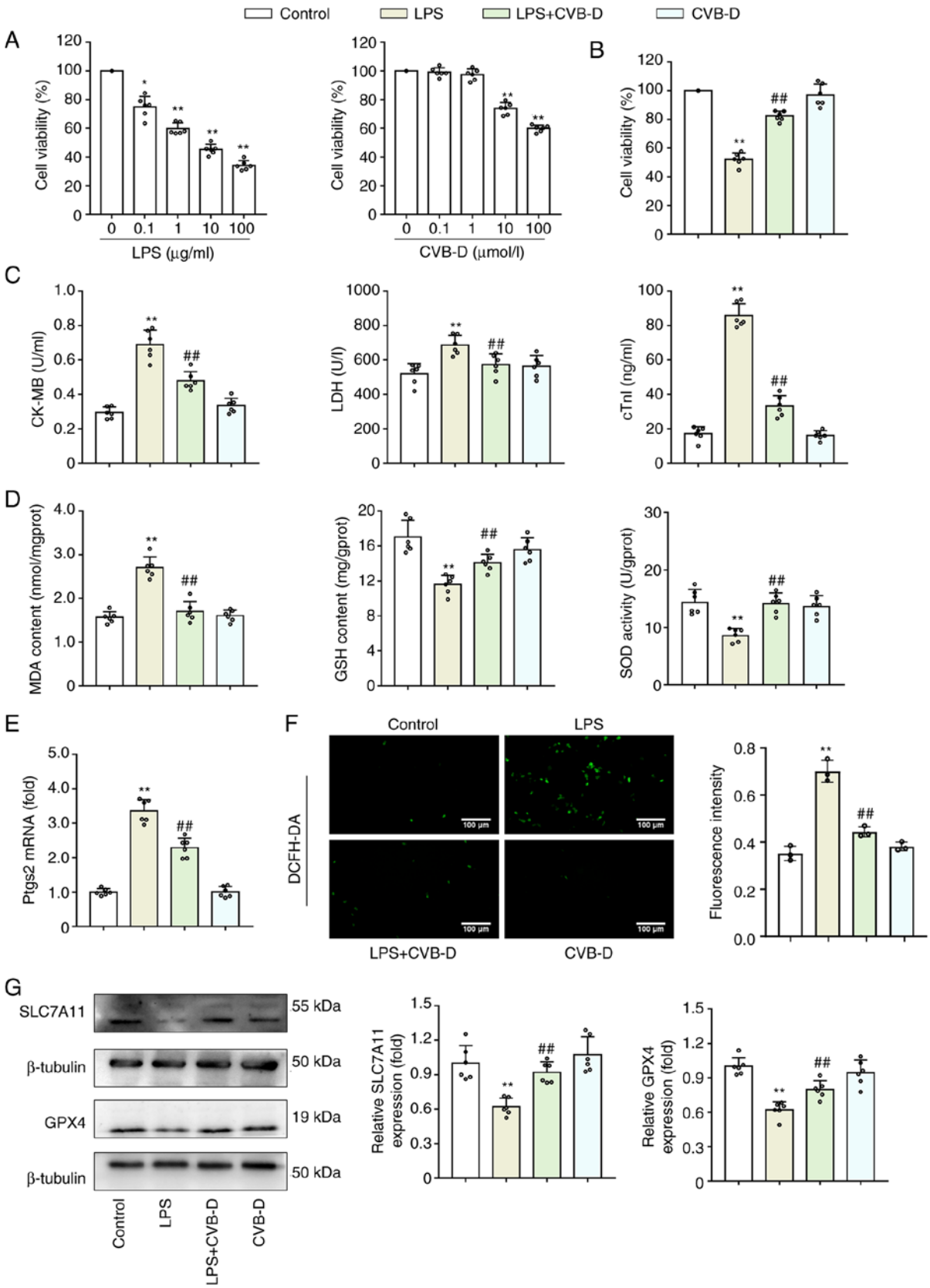

Figure 1. CVB-D exerts a protective effect on LPS-treated H9C2 cells by inhibiting ferroptosis. (A) CCK-8 assay was used to determine the dose of CVB-D and LPS for further study. (B) Effect of CVB-D on LPS-treated H9C2 cell viability. (C) Effect of CVB-D on CK-MB levels, LDH activity and cTnI levels of LPS-treated H9C2 cells. (D) Effect of MDA generation, GSH levels and SOD activity in LPS-treated H9C2 cells. (E) Effect of CVB-D on the expression of *ptgs2* mRNA levels (n=3). (F) Representative fluorescent microscopy images of ROS production by H9C2 cells (n=3). (G) SLC7A11 and GPX4 protein expression levels of LPS- and CVB-D-treated H9C2 cells. Western blot images were taken from different gels but a single replicate. *P<0.05 vs. control group, **P<0.01 vs. control group, $^{\#\#}$P<0.01 vs. LPS-treated group. Data are presented as the mean ± SD (n=6). CVB-D, cyclovirobuxine D; LPS, lipopolysaccharide; CK-MB, creatine kinase isoenzyme; LDH, lactate dehydrogenase; cTnI, cardiac troponin I; SOD, superoxide dismutase; GSH, glutathione; MDA, malondialdehyde; ptgs2, prostaglandin-endoperoxide synthase 2; ROS, reactive oxygen species; DCFH-DA, 2',7'-dichlorofluorescein diacetate; SLC7A11, solute carrier family 7 member 11; GPX4, glutathione peroxidase 4; CCK-8, Cell Counting Kit-8.

reduced GSH levels and significantly increased SOD activity; however, CVB-D significantly reversed these effects (Fig. 1D). The enhancement of ptgs2 mRNA is used as a putative marker of ferroptosis (9). CVB-D pretreatment significantly reduced the stimulatory effects of LPS on ptgs2 mRNA ($P<0.01$) (Fig. 1E). ROS production was analyzed using the ROS sensitive DCFH-DA probe. The images from this experiment demonstrated that LPS-treated H9C2 cells generated increased ROS compared with controls. CVB-D significantly decreased the ROS generation induced by LPS (Fig. 1F). Since the SLC7A11-GSH-GPX4 antioxidant axis is important in ferroptosis, the protein expression levels of SLC7A11 and GPX4 were analyzed in LPS-induced H9C2 cells pretreated with CVB-D. The protein expression levels of SLC7A11 and GPX4 were significantly reduced after LPS treatment but were elevated by treatment with CVB-D (Fig. 1G).

CVB-D inhibits LPS-induced iron overload. Excess cellular iron has been previously reported to promote the generation of both soluble and lipid ROS via the Fenton reaction, which favors the ferroptotic effect (27). Thus, it was hypothesized that CVB-D inhibited oxidative stress, lipid peroxidation and ferroptosis by modulating the abnormal iron metabolism induced by LPS. In the LPS-treated group of H9C2 cells, the significant decrease in calcein fluorescence intensity indicated a high level of calcein-bound iron, while CVB-D pretreatment significantly reversed this change (Fig. 2A). In addition, the presence of iron transporter proteins, such as DMT1, TfR1, FPN1 and FtH, was detected by western blotting (Fig. 2B). Compared with the LPS-treated group, CVB-D treatment significantly reduced DMT1, TfR1 and FtH protein expression levels but significantly increased FPN1 protein expression levels, which suggested that CVB-D may suppress iron uptake and storage while increasing iron export. As FPN1 is the only known iron exporter in mammalian cells, the expression levels of hamp mRNA. The stimulation of LPS in cells has been reported to induce the release of many inflammatory cytokines. Indeed, compared with the LPS group, CVB-D pretreatment significantly decreased the levels of *hamp* mRNA in H9C2 cells (Fig. 2C). Compared with LPS-treated cells, CVB-D pretreatment significantly decreased the protein expression levels of pro-IL-1β, TNF-α and IL-6 and the p-STAT3/STAT3 ratio in H9C2 cells (Fig. 2D). These findings demonstrated that CVB-D treatment could significantly inhibit iron-overload by modulating iron metabolism. In particular, CVB-D could eliminate LPS-induced hepcidin by blocking of the IL-6/STAT3 axis.

CVB-D protects against LPS-induced ferroptosis in H9C2 cells by upregulating Nrf2. Nrf2 has previously been reported to promote intracellular iron accumulation by downregulating FPN1 (28). To confirm whether Nrf2 serves an important role in protecting cells from septic harm, H9C2 cells were treated with the Nrf2 inhibitor ML385 at a dose of 1 μM/l for 12 h. Nrf2, SLC7A11 and GPX4 protein expression levels in H9C2 cells were analyzed (Fig. 3A). LPS significantly downregulated Nrf2 expression, and Nrf2 expression was significantly increased when LPS was combined with CVB-D treatment (Fig. 3B). Therefore, the hypothesis that an enhancement of Nrf2 would be harmful to cells by increasing iron by downregulating FPN1 was not supported. SLC7A11 and GPX4 protein expression levels were significantly upregulated in septic cells pretreated with CVB-D compared with controls, while ML385 significantly reversed this change (Fig. 3C and D). This indicated that Nrf2 serves a role in the protective effects of CVB-D against ferroptosis, but not via FPN1.

CVB-D attenuates myocardial injury induced by CLP surgery in rats. To evaluate whether CVB-D was beneficial for septic heart injury, cardiac structure and function in rats were assessed. H&E staining demonstrated that CVB-D treatment reduced the myocardial tissue damage caused by CLP (Fig. 4A). The rats in the CLP surgery group exhibited marked cardiomyocyte disorders, myocardial abnormalities, inflammatory cell infiltration, visible fibrosis and fiber breakage compared with the control surgery group. In contrast, the rats in the CLP surgery group pretreated with CVB-D demonstrated no obvious inflammatory cell infiltration or fibrosis and the arrangement of myocardial fibers was neat. Serum levels of CK-MB, LDH and cTnI, consistent with the degree of myocardial cell injury, were significantly increased in the myocardium of CLP rats compared with controls (Fig. 4B). Furthermore, CVB-D pretreatment significantly inhibited CLP-induced increases in CK-MB, LDH and cTnI (Fig. 4B). Type M-mode sonograms were performed to measure left ventricular function (Fig. 1C). The left ventricular ejection fraction shortening fraction was significantly decreased in the CLP-treated group compared with the control group (Fig. 4D). LVESV and LVDEV were both significantly increased in the CLP-treated group compared with the control. This change was significantly reversed in the CLP + CVB-D treatment group, but no significant differences were observed between the CVB-D group and the control. This suggested that CVB-D demonstrated a significant ameliorative effect on left ventricular dysfunction caused by CLP surgery.

CVB-D reduces myocardial ferroptosis induced by CLP surgery in rats. To evaluate whether ferroptosis was involved in the cardioprotective effect of CVB-D on septic heart injury, levels of ferroptosis related markers were examined in myocardial tissues. TEM was used to image the ultrastructure of myocardial mitochondria (Fig. 5A). In the control group, the mitochondrial membrane was complete and the cristae were clear. Cardiomyocytes in the CLP-treated rats demonstrated some shrunken mitochondria with solidified mitochondrial membranes and decreased mitochondrial cristae. Pretreatment with CVB-D prevented these changes to mitochondrial ultrastructure, while CVB-D did not change the mitochondrial ultrastructure in control rats (Fig. 5A). Prostaglandin-endoperoxide synthase 2 (PTGS2) is considered a biomarker of ferroptosis (29). The significant CLP-induced increase in *ptgs2* mRNA expression levels compared with controls, was significantly reversed by CVB-D pretreatment (Fig. 5B). Moreover, CVB-D attenuated sepsis-induced lipid peroxidation, as demonstrated by the significant decrease in MDA levels and the significant increase in GSH levels (Fig. 5C and D). Analysis of non-heme iron levels demonstrated that CVB-D prevented ferroptosis by inhibiting septic iron-overload (Fig. 5E). CVB-D intervention

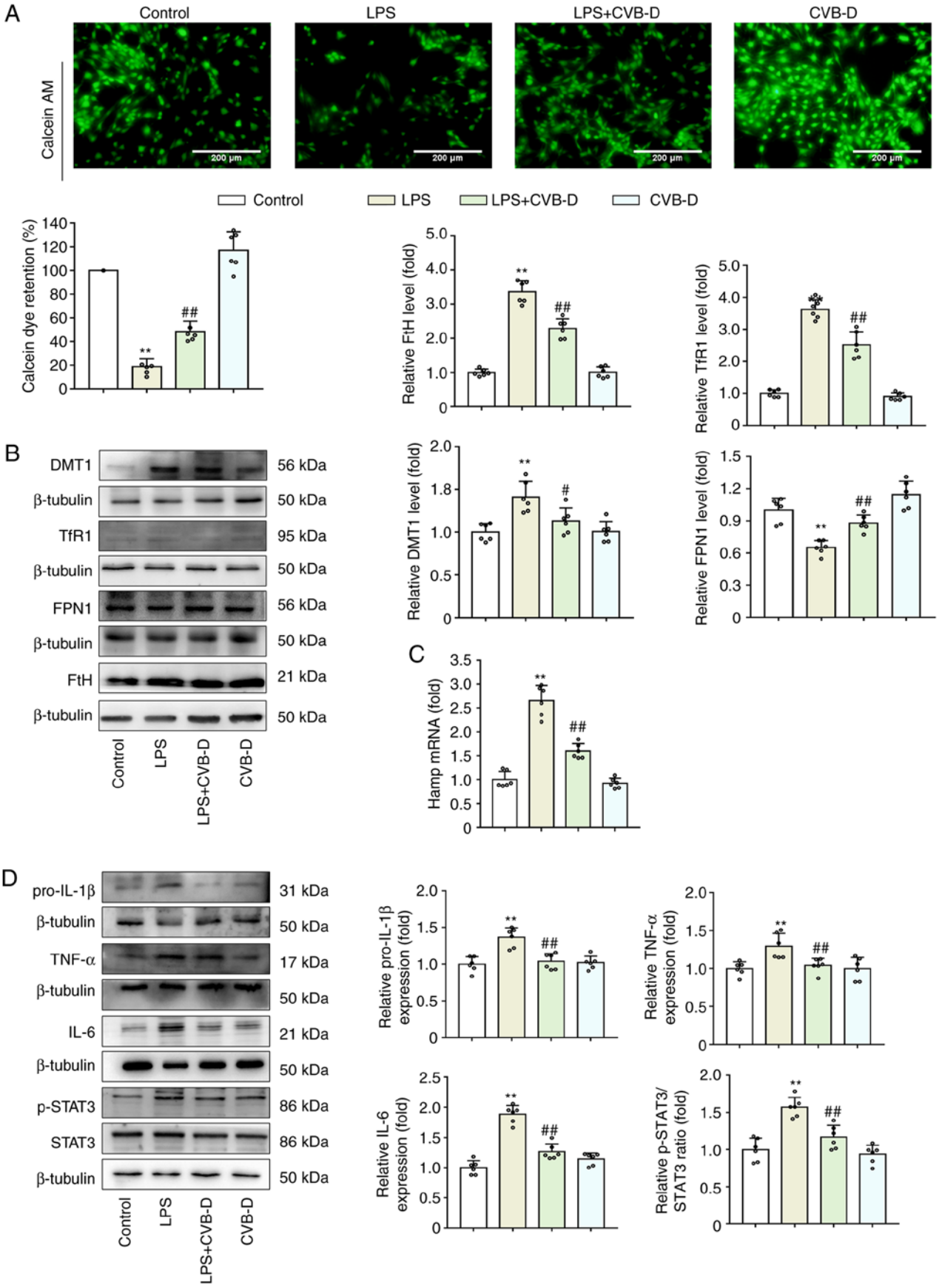

Figure 2. CVB-D inhibits cellular iron-overload induced by LPS. (A) Calcein-AM imaging of intracellular iron levels in H9C2 cells. (B) Western blot images and protein expression levels of DMT1, TfR1, FPN1 and FtH in LPS- and CVB-D-treated H9C2 cells. (C) *hamp* mRNA expression levels in LPS- and CVB-D-treated H9C2 cells. (D) Protein expression levels of pro-IL-1β, TNF-α, IL-6, p-STAT3 and STAT3 in LPS- and CVB-D-treated H9C2 cells. Data are presented as the mean ± SD (n=6). **P<0.01 vs. control group, $^{\#}$P<0.05, $^{\#\#}$P<0.01 vs. LPS-treated group. Western blot images were from different gels, but the same replicate. CVB-D, cyclovirobuxine D; LPS, lipopolysaccharide; hamp, hepcidin; DMT1, divalent metal transporter 1; TfR1, transferrin receptor 1; FPN 1, ferroportin1; IL, interleukin; TNF-α, TNF tumor necrosis factor-α; STAT3, signal transducer and activator of transcription 3; p, phosphorylated.

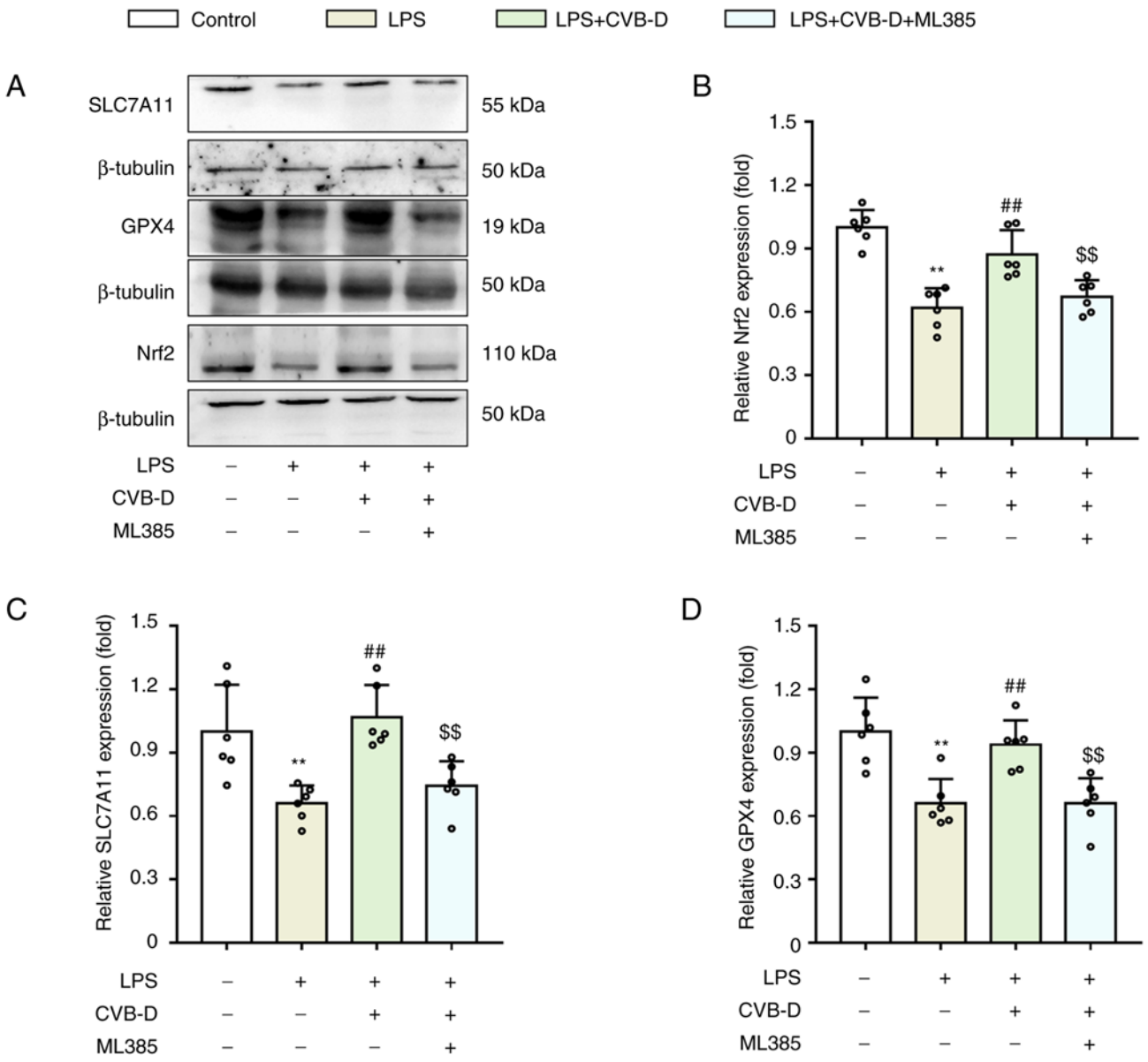

Figure 3. CVB-D protects against LPS-induced ferroptosis in H9C2 cells by upregulating Nrf2 expression. (A) Western blot images of protein levels of H9C2 cells treated with LPS and CVB-D. (B) Nrf2 protein expression levels in H9C2 cells treated with LPS and CVB-D. (C) SLC7A11 protein expression levels in H9C2 cells treated with LPS and CVB-D. (D) GPX4 protein expression levels in H9C2 cells treated with LPS and CVB-D. **P<0.01 vs. control group, $^{\#\#}$P<0.01 vs. LPS-treated group, $^{\$\$}$P<0.01 vs. LPS + CVB-D-treated group. Data are presented as the mean ± SD (n=6). Western blot images are from different gels but the same replicate. CVB-D, cyclovirobuxine D; LPS, lipopolysaccharide; SLC7A11, solute carrier family 7 member 11; Nrf2, nuclear factor erythroid 2-related factor 2; GPX4, glutathione peroxidase 4.

downregulated the liver *hamp* mRNA expression levels in CLP-treated rats (Fig. 5F). These changes indicated that CVB-D pretreatment effectively inhibited cardiac ferroptosis in septic rats. To determine whether ferroptosis was closely related to the pathophysiological processes of septic heart injury, pretreatment with Ferr-1 was applied before CLP surgery. It was subsequently demonstrated that inhibition of ferroptosis could significantly elevate both ejection fraction and fractional shortening compared with the CLP-treated group (Fig. 5G).

CVB-D alleviates the calcium overload caused by LPS in H9C2 cells. LTCCs and T-type calcium channels also serve a role in iron uptake into the heart (30). Therefore, the present study further analyzed the effect of CVB-D on calcium channels in septic cells. The influx of calcium ions was analyzed by detecting the fluorescence intensity of Ca^{2+} using Fluo-4 AM staining. The intracellular Ca^{2+} concentration was markedly increased after LPS stimulation compared with the control (Fig. 6A). Intracellular calcium levels were markedly reduced by CVB-D treatment.

CVB-D reduces L-type Ca^{2+} currents ($I_{Ca\text{-}L}$) and myocyte contraction. Calcium channels are ion channels which selectively allow for the passage of calcium ions. Voltage-gated calcium channels and ligand-gated calcium channels are two categories of calcium channels. Voltage-gated channels include L-type, T-type and N-type calcium channels. LTCCs are the main source of inward calcium flow in cardiac myocytes (31).

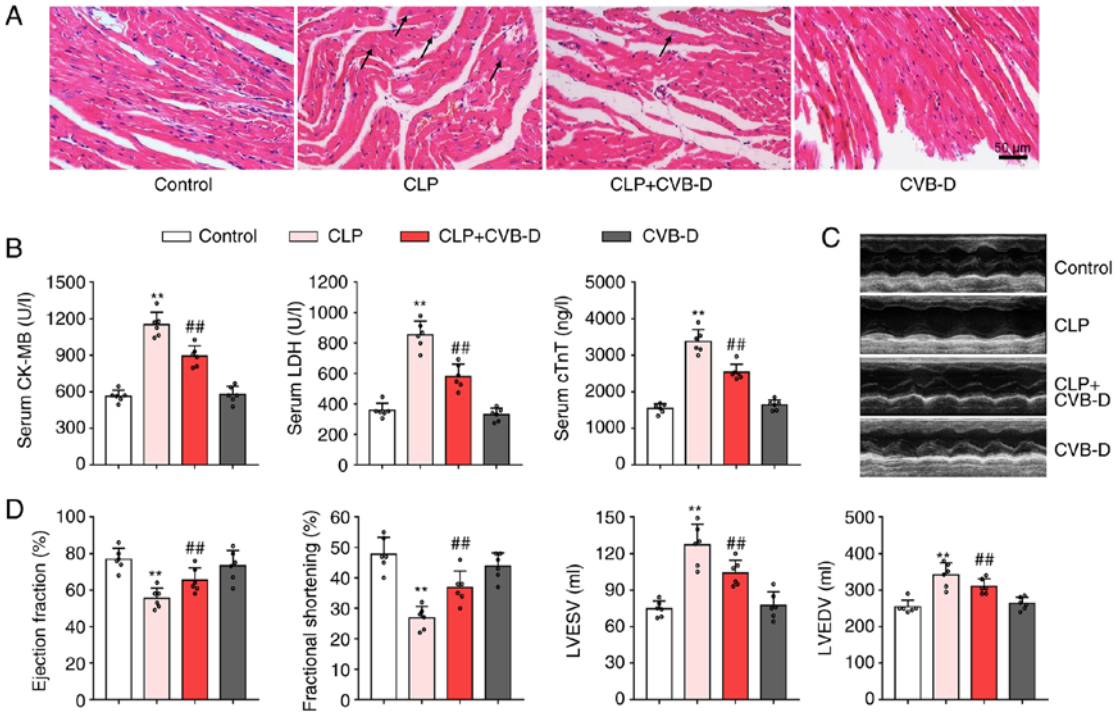

Figure 4. Protective effect of CVB-D on cardiac injury after CLP. (A) Representative histopathological images indicating myocardial tissue damage. Arrows indicate swollen cardiomyocytes and inflammatory infiltrating cells. (B) Serum levels of CK, LDH and cTnI in rats treated with CLP and CVB-D. (C) Representative echocardiographic images of rats treated with CLP and CVB-D. (D) Left ventricular ejection fraction, shortening fraction, left ventricular end-systolic volume and left ventricular end-diastolic volume of rats treated with CLP and CVB-D. Data are presented as the mean ± SD (n=6). **P<0.01 vs. control group, $^{\#\#}$P<0.01 vs. CLP group. CVB-D, cyclovirobuxine D; CLP, cecal ligation and puncture; CK-MB, creatine kinase isoenzyme; LDH, lactate dehydrogenase; cTnI, cardiac troponin I; LVESV, left ventricular end-systolic volume; LVDEV, left ventricular end-diastolic volume.

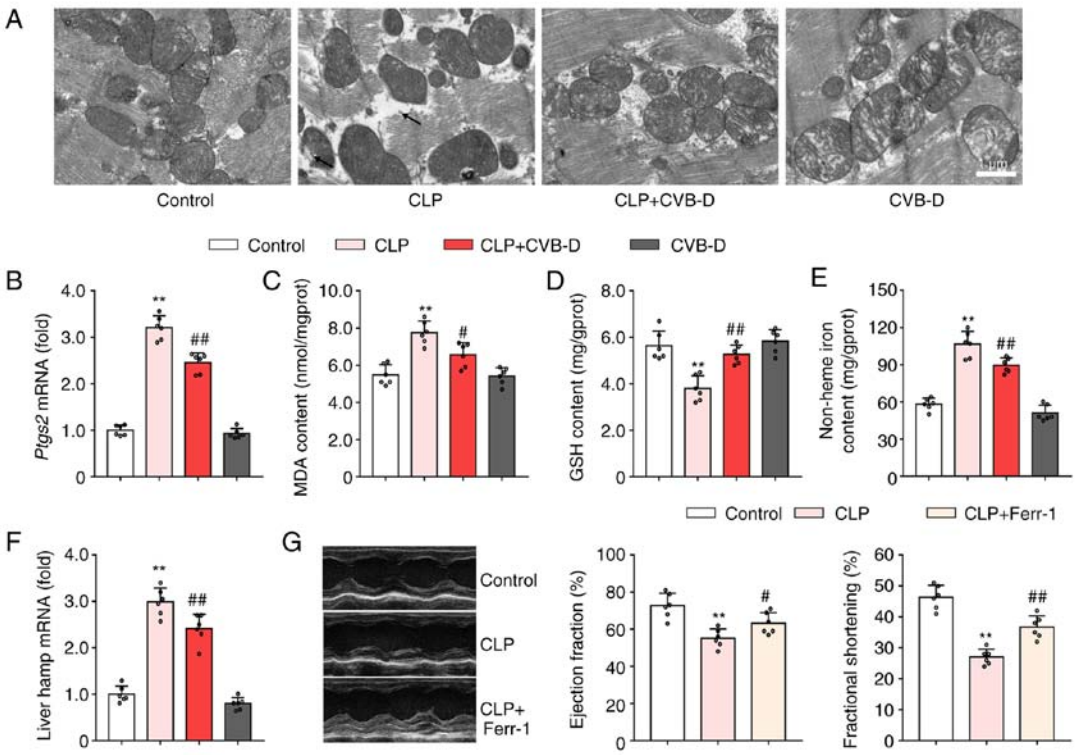

Figure 5. CVB-D reduces myocardial ferroptosis induced by CLP surgery in rats. (A) Representative TEM images showing myocardial mitochondria ultrastructure. (B) mRNA expression levels of ptgs2 in hearts of rats treated with CLP and CVB-D. (C) MDA levels in hearts of rats treated with CLP and CVB-D. (D) GSH levels in hearts of rats treated with CLP and CVB-D. (E) Levels of cardiac non-heme iron content in hearts of rats treated with CLP and CVB-D. (F) mRNA expression levels of *hamp* in livers of rats treated with CLP and CVB-D. (G) Representative echocardiographic images, and left ventricular ejection fraction and shortening fraction of CLP- and Ferr-1-treated rats. Data are presented as the mean ± SD (n=6). **P<0.01 vs. control group, $^{\#}$P<0.05, $^{\#\#}$P<0.01 vs. CLP-treated group. CVB-D, cyclovirobuxine D; CLP, cecal ligation and puncture; PTGS2, prostaglandin-endoperoxide synthase 2; *hamp*, hepcidin; SOD, superoxide dismutase; GSH, glutathione; MDA, malondialdehyde.

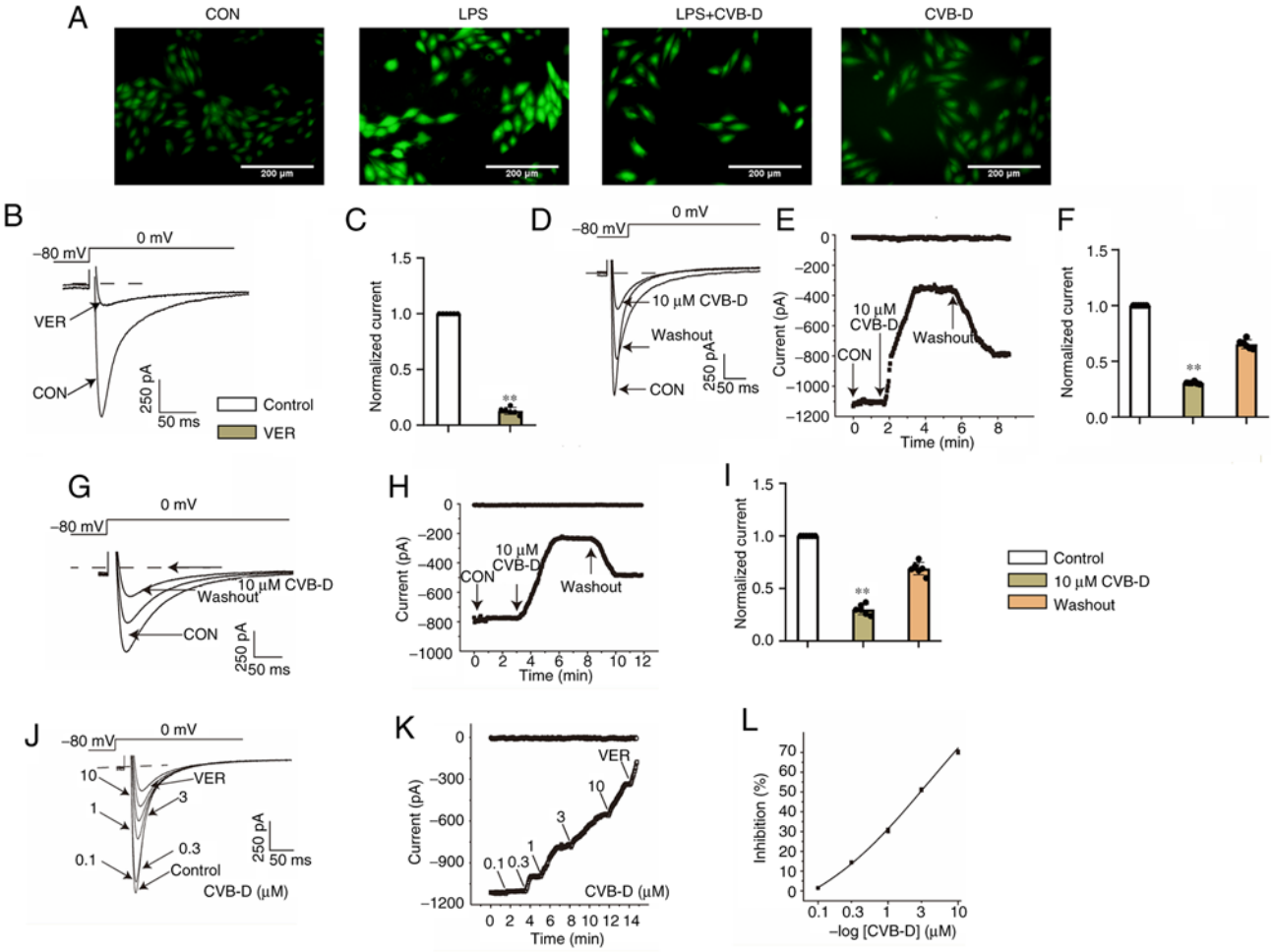

Figure 6. CVB-D attenuates calcium overload caused by LPS. (A) Fluorescence microscopy image of different treatment groups of H9C2 cells: CON, LPS, LPS + CVB-D and CVB-D. (B) Exemplary trace and (C) summary data of ICa-L recordings of VER. (D) Typical traces of normal cells. (E) Time course of $I_{Ca\text{-}L}$ in normal cells. (F) Pooled data recorded normal cells under CON, 10 μM CVB-D and washout conditions. (G) Typical traces of the CLP group cells. (H) Time course of $I_{Ca\text{-}L}$ in the CLP group cells. (I) Pooled data recorded the CLP group cells under CON, 10 μM CVB-D and washout conditions. (J) Exemplary traces and (K) time course of $I_{Ca\text{-}L}$ exposure to 0.1, 0.3, 1, 3 and 10 μM CVB-D and 1 μM VER were recorded. (L) Dose-response curves show that CVB inhibited $I_{Ca\text{-}L}$ in ventricular myocytes. **P<0.01 vs. control group. Data are presented as the mean ± SD (n=6). CON, control; CVB-D, cyclovirobuxine D; LPS, lipopolysaccharide; VER, verapamil; ICa-L, L-type Ca^{2+} current.

Measurement of $I_{Ca\text{-}L}$. VER (1 μM), a specific L-type calcium current blocker, almost completely blocked LTCC, which indicated that the flowing current was Ca^{2+} current. Partial recovery of LTCC was observed after external fluid administration (Fig. 6B and C).

CVB-D inhibits $I_{Ca\text{-}L}$ currents in normal and ischemic cardiomyocytes. During CVB-D (10 μM) exposure, $I_{Ca\text{-}L}$ decreased significantly, by 69.43±0.42%. The partial recovery of $I_{Ca\text{-}L}$ after topical solution washing indicated that the effect of CVB-D on $I_{Ca\text{-}L}$ was reversible (Fig. 6D-F). The peak amplitude of $I_{Ca\text{-}L}$ in CLP group ventricular myocytes was reduced by 70.22±1.98% at 10 μM CVB-D. The L-type Ca^{2+} current was partially recovered after the current was stabilized using an external solution, which indicated that CVB-D inhibited $I_{Ca\text{-}L}$ in normal and post-infected rat ventricular myocytes with a partially reversible effect (Fig. 6G-I).

CVB-D concentration-dependent inhibition of $I_{Ca\text{-}L}$. The current trajectories from the test of potential depolarization from -80 mV to 0 mV under the action of various concentrations of CVB-D were analyzed (Fig. 6J). With increasing CVB-D concentrations (0.1-10 μmol/l), $I_{Ca\text{-}L}$ was gradually inhibited. CVB-D (10 μM) significantly decreased $I_{Ca\text{-}L}$ in normal cells and LPS-treated ventricular myocytes by increasing the concentration of CVB-D, and the time course of $I_{Ca\text{-}L}$ was gradually decreased (Fig. 6K). The time dependence of CVB-D on $I_{Ca\text{-}L}$ was measured (Fig. 6L). The inhibition rates of CVB-D at 0.1, 0.3, 1, 3 and 10 μM were 1.48±0.12, 14.41±0.76, 30.51±1.15, 51.09±0.96 and 72.04±1.31%, respectively.

Effect of CVB-D on the I-V relationship of $I_{Ca\text{-}L}$. The current-voltage curves of the control and 0.1, 0.3, 1, 3 and 10 μM CVB-D and VER (1 μM) treatment groups recorded during the steady-state activation procedure were measured (Fig. 7A). Potentials from -60-60 mV were measured at different treatment concentrations and a representative trace was generated. In addition, CVB-D demonstrated a marked dose-dependent effect on the current-voltage (I-V) curve (Fig. 7B).

Effects of CVB-D on the homeostatic activation and inactivation of $I_{Ca\text{-}L}$. The effect of CVB-D concentrations (1 and 10 μmol/l) on the steady-state activation caused a significant left shift and inactivation curve did not change significantly. In the $I_{Ca\text{-}L}$ activation and inactivation curves, CVB-D caused a marked leftward movement.

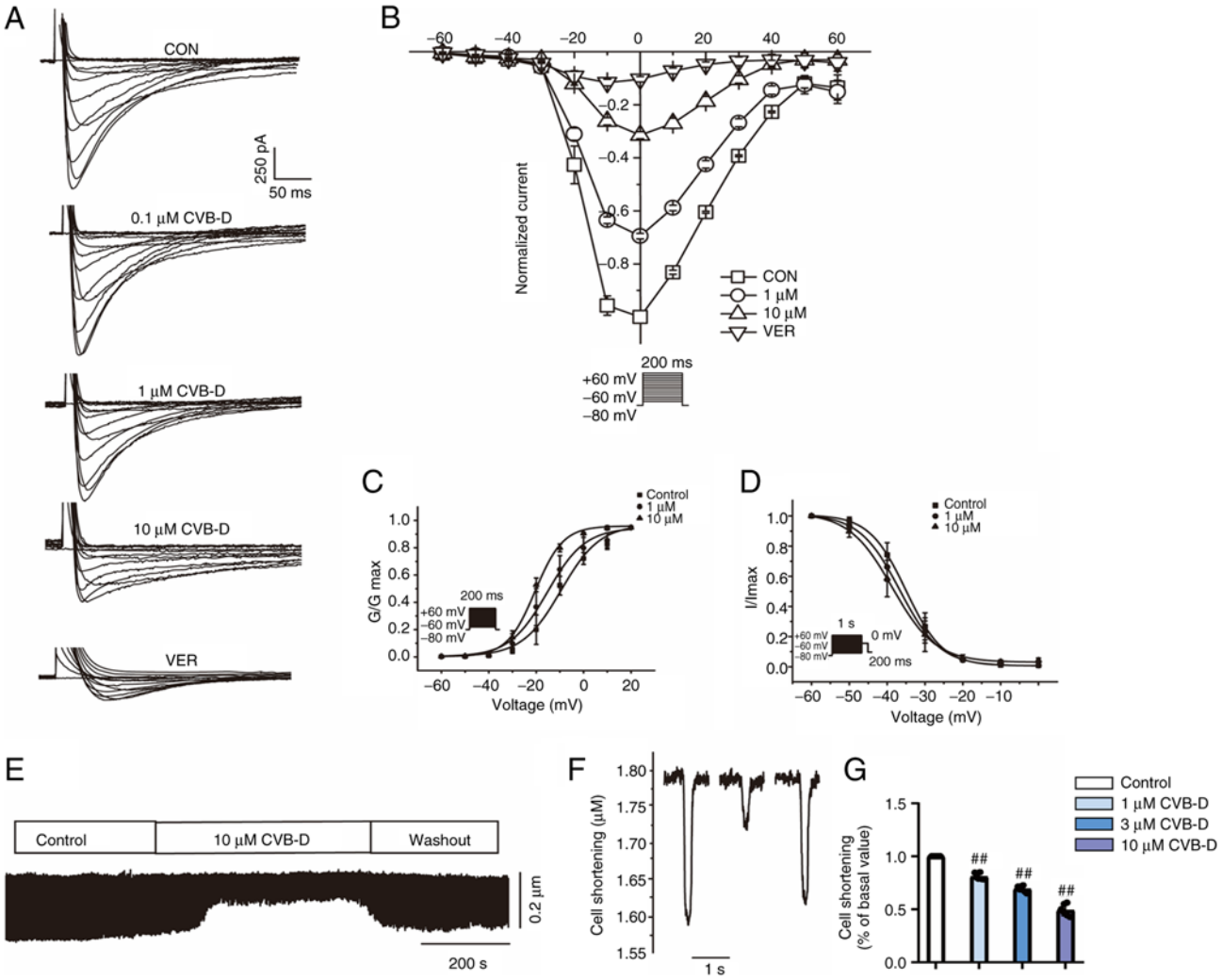

Figure 7. Impact of CVB-D on the current-voltage relationship of $I_{Ca\text{-}L}$. The test voltage is on the X-axis and the current density is on the Y-axis (pA/pF). (A) Representative traces and (B) pooled data demonstrate the impact of CVB-D at different concentrations on the I-V relationship. Effects of CVB-D on (C) steady-state activation and (D) inactivation of L-type Ca^{2+} currents. (E) Recordings of the process of cardiomyocytes shortening. (F) A single typical trace recorded in CON, 10 μM CVB-D and without CVB-D. (G) Summarized data were counted under CON, 1 μM CVB-D, 3 μM CVB-D and 10 μM CVB-D. Data are expressed as mean ± SD (n=6). $^{\#\#}$P<0.01 vs. control group CVB-D, cyclovirobuxine D; I-V, current-voltage; CON, control; VER, verapamil; $I_{Ca\text{-}L}$, L-type Ca^{2+} current.

The V2/1 value/slope factor (k) of activated CON and CVB-D (1 and 10 μmol/l) were -9.685±1.774/8.880±1.631, -15.609±1.565/8.541±1.486 and -20.646±0.7345/6.1189±0.668, respectively (Fig. 7C). The V2/1/slope factor (k) values of the inactivation curves in CON and CVB-D (from 1 and 10 μmol/l) were -35.037±0.066/4.831±0.054, -36.649±0.091/5.333±0.080 and -38.624±0.262/5.712±0.241, respectively (Fig. 7D).

CVB-D inhibits ventricular myocyte contractility. Recordings of the process of cardiomyocyte shortening were performed (Fig. 7E) and the effect of CVB-D treatment (10 μmol/l) on myocyte shortening was analyzed (Fig. 7F). CVB-D significantly inhibited myocyte shortening by 48.87±5.44%. After washing out, the contractility partially returned (Fig. 7G).

Discussion

Sepsis-derived lesions can involve numerous organs, including the heart and kidneys (32). SC is an important link in the process of multiple organ dysfunction syndrome. In previous years, numerous active ingredients have improved myocardial injury caused by sepsis through various mechanisms (33). For instance, luteolin increases autophagy through adenosine 5'-monophosphate-activated protein kinase (AMPK) signaling, thereby ameliorating LPS-induced myocardial injury (34), Ferr-1 alleviates sepsis-induced cardiac dysfunction through the toll-like receptor 4//NF-κB signaling pathway (35) and puerarin prevents iron deposition by acting on the AMPK signaling pathway and protecting the myocardium from LPS-induced injury (36). Proinflammatory cytokines act synergistically to reduce myocardial contractility. And ROS-induced oxidative stress-mediated mitochondrial damage accelerates mitochondrial malfunction, improves cardiac function and reduces mortality (37). Although much progress has been made in understanding the mechanisms underlying this disease, clinically available treatments are still limited, and thus, finding new drugs for the treatment of SC is important.

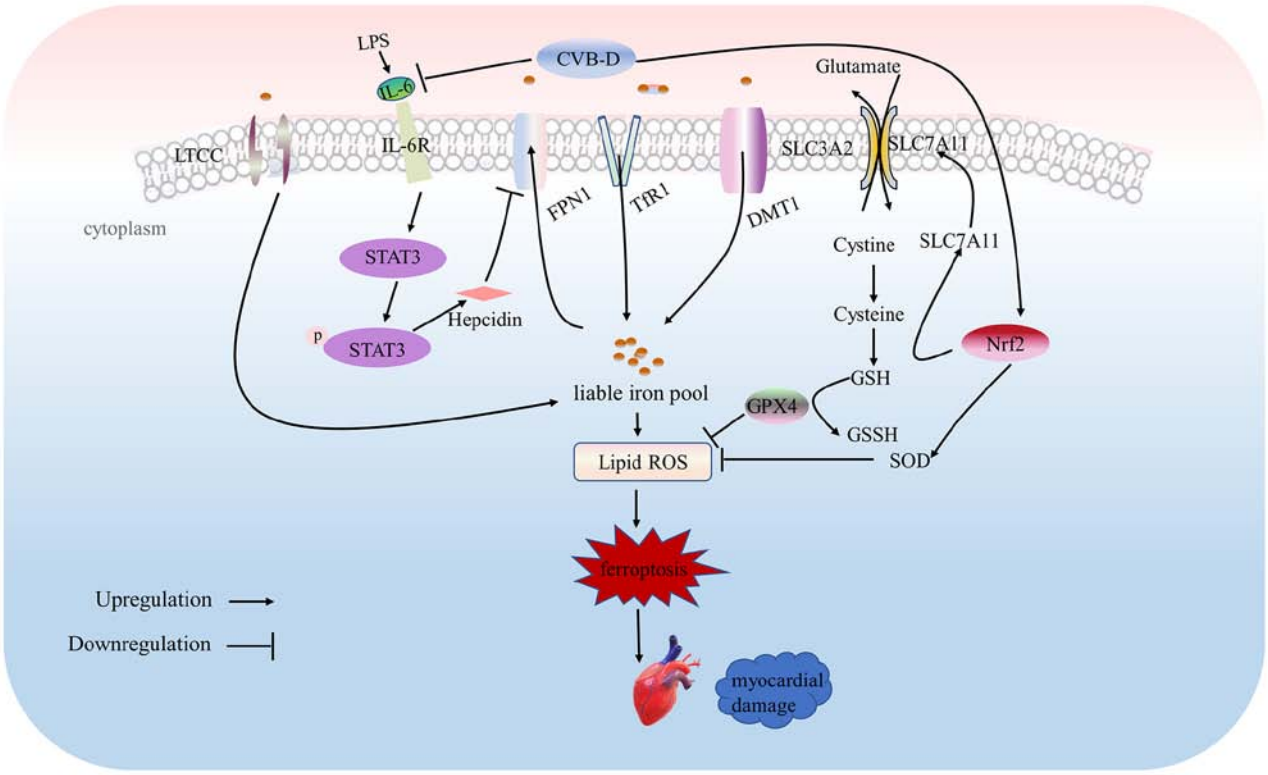

Figure 8. Proposed signaling pathways involved in the protective effect of CVB-D in septic cardiomyopathy. Cellular injury, ferroptosis and oxidative stress induced by LPS are attenuated by CVB-D. CVB-D downregulated cellular iron accumulation by alleviating cellular inflammatory responses. Furthermore, CVB-D also upregulated the Nrf2/SLC7A11/GPX4 pathway. CVB-D may reduce the influx of calcium ions by inhibiting LTCCs, thus reducing myocardial injury. CVB-D, cyclovirobuxine D; LPS, lipopolysaccharide; LTCCs, L-type calcium channels; SLC7A11, solute carrier family 7 member 11; Nrf2, nuclear factor erythroid 2-related factor 2; GPX4, glutathione peroxidase 4; ROS, reactive oxygen species; p, phosphorylated; IL, interleukin; R, receptor; SLC3A2, solute carrier family 3 member 2; STAT3, signal transducer and activator of transcription 3; FPN1, ferroportin 1; TfR1, transferrin receptor 1; DMT1, divalent metal transporter 1; GSH, glutathione; GSSH, glutathione disulfide, SOD, superoxide dismutase.

CVB-D is utilized in China in the prevention and therapy of a variety of cardiovascular dysfunction-related disorders including angina pectoris, coronary heart disease, arrhythmia and heart failure (38). CVB-D has been reported to protect against diabetic cardiomyopathy by triggering Nrf2-mediated antioxidant responses (16). It has also been reported to improve the anti-inflammatory response in LPS-stimulated mouse macrophages (39). In the present study, it was hypothesized that CVB-D may protect the myocardium from LPS-induced damage by inhibiting oxidative stress. Inflammation is the initial biological process associated with SC and is a hallmark for the development of SC (40). TNF-α, IL-6 and IL-1β are major inflammatory mediators, which are overproduced in sepsis (41). The present study demonstrated that CVB-D reduced the transcription levels of inflammatory mediators TNF-α, IL-6 and IL-1β in LPS-stimulated cardiomyocytes. In addition, the overproduction of ROS caused lipid oxidation, further compromising cellular integrity. CVB-D has been reported to play an anti-oxidative stress role in in cardiomyocytes (42). Therefore, the present study measured the protein expression levels of the cysteine/glutamate transporter SLC7A11, which is the main source of cysteine used for synthesizing glutathione, and of the lipid hydroperoxidase GPX4, which serves an important role in eliminating lipid peroxidation (43). Therefore, CVB-D may alleviate myocardial injury by regulating ferroptosis in H9C2 cells.

Ferroptosis is a highly iron-dependent and lipid peroxidation-driven form of cell death (44). Ferroptosis is essential for the physiological function of biological systems through the involvement of iron in various pathways such as iron metabolism, oxidative stress and lipid peroxidation (45). In a state of oxidative stress, superoxide is produced over a short period of time, reducing ferric iron stored in ferritin (composed of FtH and FtL) to ferrous iron and leading to its release from the cell (45). DMT1 and TFR1 act as an 'on' switch for cellular iron homeostasis to take up extracellular iron into the cell, and FPN1 acts as an 'off' switch in the system responsible for exporting excess iron from inside to outside of the cells (44). The results of the present study demonstrated that CVB-D treatment significantly reduced intracellular iron content. Hepcidin is a hormone that serves a crucial role in iron homeostasis management (46). STAT3 has previously been identified as a critical transcription factor involved in the stimulation of iron-regulated hormone expression of genes in the liver by IL-6 (47). The findings of the present study support that CVB-D reduces intracellular iron by suppressing inflammation and decreasing hepcidin transcription produced by the IL-6/STAT3 pathway, enhancing iron release.

To further investigate the results observed in the present study, production of ferroptosis-related proteins was measured. GPX4, a member of the GPX protein family, serves a key role as a critical regulator in ferroptosis, mainly through

the inhibition of lipid peroxide formation (48). System xc^- is located in phospholipid duplexes and serves as an important part of the cellular antioxidant system, comprising SLC7A11 and SLC3A2 (49). Inhibition of system xc^- activities influences GSH synthesis by inhibiting cystine uptake, which leads to decreased GPX activity, reduced cellular antioxidant capacity and lipid peroxidation accumulation, resulting in oxidative damage and ferroptosis (50). As demonstrated in the present study, the group of LPS-treated H9C2 cells expressed lower levels of GPX4 and SLC7A11 and CVB-D prevented this impact, which indicated that ferroptosis is implicated in the development of SC and CVB-D suppresses ferroptosis.

Nrf2 is considered to be a key regulator of resistance to oxidative stress and a number of its downstream targets serve critical roles in redox homeostasis (51), during which it impacts the expression of SLC7A11 and GPX4 (52). The present study demonstrated that CVB-D increased Nrf2 in LPS-treated H9C2 cells, which indicated that CVB-D triggered the translocation of Nrf2; however, the Nrf2 inhibitor ML385 decreased this effect of CVB-D on GPX4 and SLC7A11 levels in LPS-treated H9C2 cells. The results from the present study suggest that CVB-D activated the Nrf2/SLC7A11/GPX4 signaling axis in LPS-treated H9C2 cells.

Previous studies have reported that calcium serves a critical role in regulating ferroptosis through several pathways (53). It has been reported that excess Ca^{2+} levels increase calpain protease activity, which is responsible for cleaving BH3-interacting domain death agonist and apoptosis-inducing factor, two proteins that contribute to ferroptosis (54). Moreover, elevated intracellular Ca^{2+} contributes to activated calcium-dependent phospholipase A2, which promotes arachidonic acid release from cell membranes and initiates ferroptosis through the accumulation of lipid peroxides after the esterification of arachidonic acid into phosphatidylethanolamines (55). In line with this notion, a recent study reported that luminal Ca^{2+} stores alter sensitivity to ferroptosis by inducing lipid remodeling, specifically by altering lipid elongation and saturation state (56). Additionally, calcium can also regulate ferroptosis by modulating the activation of the endoplasmic reticulum stress response (57). Notably, calcium can lead to an increase in ROS by affecting the electron transport chain and regulating oxidative phosphorylation (58). Thus, in turn, lipid peroxidation is promoted and ferroptosis is triggered (59). Understanding how calcium regulates ferroptosis could provide potential therapeutic targets for diseases associated with dysregulated cell death.

The present study demonstrated the beneficial effect of CVB-D on sepsis-induced cardiac dysfunction by decreasing ferroptosis. CVB-D may decrease sepsis-induced cardiomyocyte ferroptosis by inhibiting oxidative stress, iron overload, lipid peroxidation and the inward flow of calcium ions. Mechanistically, CVB-D inhibited LPS-induced iron overload by promoting ferroportin-mediated cellular iron release via the IL-6/STAT3/hepcidin axis. Furthermore, CVB-D was demonstrated to inhibit ferroptosis by activating the Nrf2/SLC7A11/GPX4 axis in cardiomyocytes, which may contribute to its protective effects against myocardial injury. Additionally, CVB-D may inhibit LTCC, thus suppressing elevated cellular calcium and iron levels. These findings emphasize the potential therapeutic value of CVB-D in the management of sepsis-induced cardiac dysfunction (Fig. 8).

CVB-D ameliorated the impairment of cardiac function induced by CLP surgery in rats. In addition, CVB-D regulated the expression of iron metabolism-related proteins in LPS-stimulated H9C2 cells and ameliorated the inflammatory response by inhibiting the IL-6/STAT3 signaling pathway and reducing the expression of hepcidin. Furthermore, in LPS-stimulated H9C2 cells, CVB-D exerted a protective effect through the Nrf2/SLC7A11/GPX4 pathway. The results of the present study are the first to report that CVB-D ameliorates ferroptosis by increasing cell survival and thus effectively ameliorates LPS-induced SC in association with activation of Nrf2/SLC7A11/GPX4 pathway targets. It was also demonstrated that CVB-D significantly reduced calcium contractility, which could be associated with inhibition of LTCCs. The present study demonstrated that CVB-D could reduce myocardial injury by inhibiting LTCCs to reduce calcium ion influx. Further *in vivo* and clinical studies are required to assess the safety and efficacy of CVB-D in SC, and to fully elucidate the mechanistic links between CVB-D treatment, ferroptosis and cardioprotection.

Acknowledgements

Not applicable.

Funding

This project was supported by the Science Foundation of Hebei Normal University (grant no. L2021B47).

Availability of data and materials

The datasets used and/or analyzed during the current study are available from the corresponding author on reasonable request.

Authors' contributions

ESJ and NW conceived and planned the study, provided supervision and obtained funding. JXW and PG collected data and drafted the manuscript. YC and MX analyzed data and reviewed and edited the manuscript. JXW and PG confirm the authenticity of all the raw data. All authors read and approved the final manuscript.

Ethics approval and consent to participate

All procedures were performed with the approval of the Animal Care and Use Committee of Hebei University of Chinese Medicine (approval no. DWLL202206006).

Patient consent for publication

Not applicable.

Competing interests

The authors declare that they have no competing interests.

References

1. Beesley SJ, Weber G, Sarge T, Nikravan S, Grissom CK, Lanspa MJ, Shahul S and Brown SM: Septic cardiomyopathy. Crit Care Med 46: 625-634, 2018.
2. Tullo G, Candelli M, Gasparrini I, Micci S and Franceschi F: Ultrasound in Sepsis and septic shock-from diagnosis to treatment. J Clin Med 12: 1185, 2023.
3. Flierl MA, Rittirsch D, Huber-Lang MS, Sarma JV and Ward PA: Molecular events in the cardiomyopathy of sepsis. Mol Med 14: 327-336, 2008.
4. Shang X, Zhang Y, Xu J, Li M, Wang X and Yu R: SRV2 promotes mitochondrial fission and Mst1-Drp1 signaling in LPS-induced septic cardiomyopathy. Aging 12: 1417-1432, 2020.
5. Zheng Z, Ma H, Zhang X, Tu F, Wang X, Ha T, Fan M, Liu L, Xu J, Yu K, *et al*: Enhanced glycolytic metabolism contributes to cardiac dysfunction in polymicrobial sepsis. J Infectious Dis 215: 1396-1406, 2017.
6. Zhu X, Sun M, Guo H, Lu G, Gu J, Zhang L, Shi L, Gao J, Zhang D, Wang W, *et al*: Verbascoside protects from LPS-induced septic cardiomyopathy via alleviating cardiac inflammation, oxidative stress and regulating mitochondrial dynamics. Ecotoxicol Environ Saf 233: 113327, 2022.
7. Yang Y, Lei W, Qian L, Zhang S, Yang W, Lu C, Song Y, Liang Z, Deng C, Chen Y, *et al*: Activation of NR1H3 signaling pathways by psoralidin attenuates septic myocardial injury. Free Radical Biol Med 204: 8-19, 2023.
8. Venkataramani V: Iron homeostasis and metabolism: Two sides of a coin. Adv Exp Med Biol 1301: 25-40, 2021.
9. Fang X, Wang H, Han D, Xie E, Yang X, Wei J, Gu S, Gao F, Zhu N, Yin X, *et al*: Ferroptosis as a target for protection against cardiomyopathy. Proc Natl Acad Sci USA 116: 2672-2680, 2019.
10. Rochette L, Dogon G, Rigal E, Zeller M, Cottin Y and Vergely C: Lipid peroxidation and Iron metabolism: Two corner stones in the homeostasis control of ferroptosis. Int J Mol Sci 24: 449, 2022.
11. Islam S, Jarosch S, Zhou J, Parquet Mdel C, Toguri JT, Colp P, Holbein BE and Lehmann C: Anti-inflammatory and anti-bacterial effects of iron chelation in experimental sepsis. J Surg Res 200: 266-273, 2016.
12. Li N, Wang W, Zhou H, Wu Q, Duan M, Liu C, Wu H, Deng W, Shen D and Tang Q: Ferritinophagy-mediated ferroptosis is involved in sepsis-induced cardiac injury. Free Radical Biol Med 160: 303-318, 2020.
13. Wang C, Yuan W, Hu A, Lin J, Xia Z, Yang CF, Li Y and Zhang Z: Dexmedetomidine alleviated sepsis-induced myocardial ferroptosis and septic heart injury. Mol Med Rep 22: 175-184, 2020.
14. National Pharmacopoeia Committee, ed. Pharmacopoeia of People's Republic of China. Beijing: Chemical Industry Press, 2010.
15. Guo Q, Guo J, Yang R, Peng H, Zhao J, Li L and Peng S: Cyclovirobuxine D attenuates doxorubicin-induced cardiomyopathy by suppression of oxidative damage and mitochondrial biogenesis impairment. Oxid Med Cell Longev 2015: 151972, 2015.
16. Jiang Z, Fu L, Xu Y, Hu X, Yang H, Zhang Y, Luo H, Gan S, Tao L, Liang G and Shen X: Cyclovirobuxine D protects against diabetic cardiomyopathy by activating Nrf2-mediated antioxidant responses. Sci Rep 10: 6427, 2020.
17. Xiang ZN, Su JC, Liu YH, Deng B, Zhao N, Pan J, Hu ZF, Chen FH, Cheng BY, Chen JC and Wan LS: Structurally diverse alkaloids from Buxus sempervirens with cardioprotective activity. Bioorg Chem 109: 104753, 2021.
18. Fang H, Gong C, Fu J, Liu X, Bi H, Cheng Y, Liu Y, Tang Y and Wang D: Evaluation of 2 rat models for sepsis developed by improved cecal ligation/puncture or feces intraperitoneal-injection. Med Sci Monitor 26: e919054, 2020.
19. Qin LY, Guan P, Wang JX, Chen Y, Zhao YS, Yang SC, Guo YJ, Wang N and Ji ES: Therapeutic potential of Astragaloside IV against adriamycin-induced renal damage in rats via ferroptosis. Front Pharmacol 13: 812594, 2022.
20. Livak KJ and Schmittgen TD: Analysis of relative gene expression data using real-time quantitative PCR and the 2(-Delta Delta C(T)) method. Methods 25: 402-408, 2001.
21. Chen DD, Wang HW and Cai XJ: Transcription factor Sp1 ameliorates sepsis-induced myocardial injury via ZFAS1/Notch signaling in H9C2 cells. Cytokine 140: 155426, 2021.
22. Xiong B, Chen L, Huang Y, Lu G, Chen C, Nong J and Pan H: ZBTB16 eases lipopolysaccharide-elicited inflammation, apoptosis and degradation of extracellular matrix in chondrocytes during osteoarthritis by suppressing GRK2 transcription. Exp Ther Med 25: 276, 2023.
23. Varghese J, James J, Vaulont S, McKie A and Jacob M: Increased intracellular iron in mouse primary hepatocytes in vitro causes activation of the Akt pathway but decreases its response to insulin. Biochim Biophys Acta Gen Subj 1862: 1870-1882, 2018.
24. Guan P, Sun ZM, Wang N, Zhou J, Luo LF, Zhao YS and Ji ES: Resveratrol prevents chronic intermittent hypoxia-induced cardiac hypertrophy by targeting the PI3K/AKT/mTOR pathway. Life Sci 233: 116748, 2019.
25. Liu L, Liu F, Sun Z, Peng Z, You T and Yu Z: LncRNA NEAT1 promotes apoptosis and inflammation in LPS-induced sepsis models by targeting miR-590-3p. Exp Ther Med 20: 3290-3300, 2020.
26. Hu X and Miao H: MiR-539-5p inhibits the inflammatory injury in septic H9c2 cells by regulating IRAK3. Mol Biol Rep 49: 121-130, 2022.
27. Cheng J, Zhu Y, Xing X, Xiao J, Chen H, Zhang H, Wang D, Zhang Y, Zhang G, Wu Z and Liu Y: Manganese-deposited iron oxide promotes tumor-responsive ferroptosis that synergizes the apoptosis of cisplatin. Theranostics 11: 5418-5429, 2021.
28. Kong Y, Hu L, Lu K, Wang Y, Xie Y, Gao L, Yang G, Xie B, He W, Chen G, *et al*: Ferroportin downregulation promotes cell proliferation by modulating the Nrf2-miR-17-5p axis in multiple myeloma. Cell Death Dis 10: 624, 2019.
29. Yang WS, SriRamaratnam R, Welsch ME, Shimada K, Skouta R, Viswanathan VS, Cheah JH, Clemons PA, Shamji AF, Clish CB, *et al*: Regulation of ferroptotic cancer cell death by GPX4. Cell 156: 317-331, 2014.
30. Kumfu S, Chattipakorn SC, Fucharoen S and Chattipakorn N: Dual T-type and L-type calcium channel blocker exerts beneficial effects in attenuating cardiovascular dysfunction in iron-overloaded thalassaemic mice. Exp Physiol 101: 521-539, 2016.
31. Hardy N, Viola HM, Johnstone VP, Clemons TD, Cserne Szappanos H, Singh R, Smith NM, Iyer KS and Hool LC: Nanoparticle-mediated dual delivery of an antioxidant and a peptide against the L-Type Ca2+ channel enables simultaneous reduction of cardiac. ACS Nano 9: 279-289, 2015.
32. Bai T, Wang S, Zhao Y, Zhu R, Wang W and Sun Y: Haloperidol, a sigma receptor 1 antagonist, promotes ferroptosis in hepatocellular carcinoma cells. Biochem Biophys Res Commun 491: 919-925, 2017.
33. Xin T and Lu C: SirT3 activates AMPK-related mitochondrial biogenesis and ameliorates sepsis-induced myocardial injury. Aging 12: 16224-16237, 2020.
34. Wu B, Song H, Fan M, You F, Zhang L, Luo J, Li J, Wang L, Li C and Yuan M: Luteolin attenuates sepsis-induced myocardial injury by enhancing autophagy in mice. Int J Mol Med 45: 1477-1487, 2020.
35. Xiao Z, Kong B, Fang J, Qin T, Dai C, Shuai W and Huang H: Ferrostatin-1 alleviates lipopolysaccharide-induced cardiac dysfunction. Bioengineered 12: 9367-9376, 2021.
36. Zhou B, Zhang J, Chen Y, Liu Y, Tang X, Xia P, Yu P and Yu S: Puerarin protects against sepsis-induced myocardial injury through AMPK-mediated ferroptosis signaling. Aging 14: 3617-3632, 2022.
37. Liu YC, Yu MM, Shou ST and Chai YF: Sepsis-induced cardiomyopathy: Mechanisms and treatments. Front Immunol 8: 1021, 2017.
38. Ke Z, Hou X and Jia XB: Design and optimization of self-nanoemulsifying drug delivery systems for improved bioavailability of cyclovirobuxine D. Drug Design Dev Ther 10: 2049-2060, 2016.
39. Guo D, Li JR, Wang Y, Lei LS, Yu CL and Chen NN: Cyclovirobuxinum D suppresses lipopolysaccharide-induced inflammatory responses in murine macrophages in vitro by blocking JAK-STAT signaling pathway. Acta Pharmacol Sinica 35: 770-778, 2014.
40. Kakihana Y, Ito T, Nakahara M, Yamaguchi K and Yasuda T: Sepsis-induced myocardial dysfunction: Pathophysiology and management. J Intensive Care 4: 22, 2016.
41. Baek HS, Min HJ, Hong VS, Kwon TK, Park JW, Lee J and Kim S: Anti-inflammatory effects of the novel PIM kinase inhibitor KMU-470 in RAW 264.7 cells through the TLR4-NF-κB-NLRP3 pathway. Int J Mol Sci 21: 5138, 2020.

42. Yu B, Fang TH, Lü GH, Xu HQ and Lu JF: Beneficial effect of Cyclovirobuxine D on heart failure rats following myocardial infarction. Fitoterapia 82: 868-877, 2011.
43. Koppula P, Zhuang L and Gan B: Cystine transporter SLC7A11/xCT in cancer: Ferroptosis, nutrient dependency, and cancer therapy. Protein Cell 12: 599-620, 2021.
44. Fang X, Ardehali H, Min J and Wang F: The molecular and metabolic landscape of iron and ferroptosis in cardiovascular disease. Na Rev Cardiol 20: 7-23, 2023.
45. Broxmeyer HE, Cooper S, Levi S and Arosio P: Mutated recombinant human heavy-chain ferritins and myelosuppression in vitro and in vivo: A link between ferritin ferroxidase activity and biological function. Proc Natl Acad Sci USA 88: 770-774, 1991.
46. Zhang H, Ostrowski R, Jiang D, Zhao Q, Liang Y, Che X, Zhao J, Xiang X, Qin W and He Z: Hepcidin promoted ferroptosis through Iron metabolism which is associated with DMT1 signaling activation in early brain injury following subarachnoid hemorrhage. Oxidative Med Cell Longevity 2021: 9800794, 2021.
47. Pietrangelo A, Dierssen U, Valli L, Garuti C, Rump A, Corradini E, Ernst M, Klein C and Trautwein C: STAT3 is required for IL-6-gp130-dependent activation of hepcidin in vivo. Gastroenterology 132: 294-300, 2007.
48. Li J, Cao F, Yin HL, Huang ZJ, Lin ZT, Mao N, Sun B and Wang G: Ferroptosis: Past, present and future. Cell Death Dis 11: 88, 2020.
49. Fotiadis D, Kanai Y and Palacín M: The SLC3 and SLC7 families of amino acid transporters. Mol Aspects Med 34: 139-158, 2013.
50. Lei P, Bai T and Sun Y: Mechanisms of ferroptosis and relations with regulated cell death: A review. Front Physiol 10: 139, 2019.
51. Dodson M, Castro-Portuguez R and Zhang DD: NRF2 plays a critical role in mitigating lipid peroxidation and ferroptosis. Redox Biol 23: 101107, 2019.
52. Ma H, Wang X, Zhang W, Li H, Zhao W, Sun J and Yang M: Melatonin suppresses ferroptosis induced by high glucose via activation of the Nrf2/HO-1 signaling pathway in type 2 diabetic osteoporosis. Oxid Med Cell Longev 2020: 9067610, 2020.
53. Dhaouadi N, Vitto VAM, Pinton P, Galluzzi L and Marchi S: Ca(2+) signaling and cell death. Cell Calcium 113: 102759, 2023.
54. Neitemeier S, Jelinek A, Laino V, Hoffmann L, Eisenbach I, Eying R, Ganjam GK, Dolga AM, Oppermann S and Culmsee C: BID links ferroptosis to mitochondrial cell death pathways. Redox Biol 12: 558-570, 2017.
55. Li D and Li Y: The interaction between ferroptosis and lipid metabolism in cancer. Signal Transduct Target Ther 5: 108, 2020.
56. Xin S, Mueller C, Pfeiffer S, Kraft VAN, Merl-Pham J, Bao X, Feederle R, Jin X, Hauck SM, Schmitt-Kopplin P and Schick JA: MS4A15 drives ferroptosis resistance through calcium-restricted lipid remodeling. Cell Death Differ 29: 670-686, 2022.
57. Fu F, Wang W, Wu L, Wang W, Huang Z, Huang Y, Wu C and Pan X: Inhalable biomineralized liposomes for cyclic Ca(2+)-Burst-centered endoplasmic reticulum stress enhanced lung cancer ferroptosis therapy. ACS Nano 17: 5486-5502, 2023.
58. Madreiter-Sokolowski CT, Thomas C and Ristow M: Interrelation between ROS and Ca(2+) in aging and age-related diseases. Redox Biol 36: 101678, 2020.
59. Peng TI and Jou MJ: Oxidative stress caused by mitochondrial calcium overload. Ann N Y Acad Sci 1201: 183-188, 2010.